Enhancement of Hot Corrosion Resistance of Modified 9Cr-1Mo Steel Through Surface Nanostructuring and Pre-oxidation

Divya Sri Bandla, Preeti Verma, Kausik Chattopadhyay, and Vakil Singh

Nanosize grains of ~ 65 nm were developed with large misorientation angles of grain boundaries in surface region of normalized and tempered modified 9Cr-1Mo steel by ultrasonic shot peening (USSP) with hard steel balls of 3 mm diameter. The surface roughness and the depth of nanostructured surface region were found to increase with the duration of USSP from 0.5 to 5 min. Hot corrosion tests were performed for the Un-USSP and the samples USSPed for the durations of 0.25 and 1.5 min and also for the samples subjected to USSP and subsequently pre-oxidation at 600 °C for 4 h. The hot corrosion resistance at 600 °C under 100% NaCl coating was significantly improved by USSP for 1.5 min and subsequent pre-oxidation at 600 °C for 4 h. The results are discussed in terms of the formation of more uniform and effective protective iron–chromium oxide layer on the USSPed surface from the subsequent pre-oxidation treatment, prior to hot corrosion of the specimens under 100% NaCl coating at 600 °C.

1. Introduction

Modified 9Cr-1Mo steel (P91) is a modified version of the conventional 9Cr-1Mo steel (P9) with the addition of strong carbide formers V and Nb which form precipitates of MX type where M stands for V and Nb and X for C and N. It is a potential candidate material for steam generator components and wrapper of fuel tube in liquid-metal-cooled fast breeder reactors (LMFBR) (Ref 1, 2) owing to combination of its good resistance against void swelling, low coefficient of thermal expansion, high thermal conductivity and microstructural stability at elevated temperatures. Microstructure of the P91 steel has been well characterized by several investigators (Ref 3-7). Thomas et al. (Ref 8) showed that size of the MX precipitates remained almost constant even after aging for 10,000 h at 873 K, in the range of service temperature. The higher microstructural stability of the P91 grade steel than that of the P9 grade was attributed to these stable MX precipitates. The high strength of this steel is mainly attributed to its typical microstructure of lath martensite with high density of dislocations and precipitates of $M_{23}C_6$ (M:Cr, Fe) and MX type in the normalized and tempered condition (Ref 9-11). During service, components of this steel in a steam generator and LMFBR undergo low cycle fatigue damage due to thermal stresses arising from startup and shutdown operations and corrosion from the liquid sodium coolant and supercritical water.

In general, fatigue, wear and corrosion resistance of a component are known to be highly sensitive to its surface microstructure and the state of the associated stress. A hard surface layer with fine-grained structure is beneficial against the damage processes referred to above. Nanosize grains at the surface of a material are induced either by surface deposition processes or by severe plastic deformation (SPD). The process of SPD has been found to be more attractive than the process of physical/chemical vapor deposition because of porosity in the nanostructure produced by the latter processes (Ref 12) which is known to be quite harmful for mechanical properties and corrosion resistance of metallic components. Ultrasonic shot peening (USSP) or surface mechanical attrition treatment (SMAT) is one of the SPD processes in which steel balls of sufficient hardness strike the surface of the component with sufficient force to induce plastic deformation and indentation. The main difference between the conventional process of shot peening (CSP) and USSP is that energy to shots is supplied by constant air flow or high-speed rotating wheel in the case of CSP, whereas in the USSP it is supplied by a sonotrode surface vibrating at a frequency of 20 kHz (Ref 13). The surface modifications induced by the process of USSP are nanostructuring (Ref 14-16), increase in the roughness and compressive residual stress (Ref 17, 18) without any change in chemical composition of the material. Increase in the roughness of the surface is deleterious to surface dependent mechanical properties like fatigue and also to corrosion resistance of metallic materials (Ref 19). However, in optimum condition of USSP process the deleterious effect of roughness is completely suppressed by the surface nanostructuring and compressive residual stress induced in the surface region. USSP causes less roughness and modifies the surface in less time, using fewer amounts of shot media than that in the process of CSP. This is because of high vibrating frequency in USSP with a large number of strikes in very short time period (Ref 20, 21).

Divya Sri Bandla, Kausik Chattopadhyay, and **Vakil Singh**, Department of Metallurgical Engineering, Indian Institute of Technology (BHU), Varanasi 221005, India; **Preeti Verma**, National Research Laboratory for Conservation of Cultural Property, Lucknow 226024, India. Contact e-mail: kausik.met@iitbhu.ac.in.

Several investigators have reported that USSP treatment in optimum operating condition enhanced fatigue resistance (Ref 22) and corrosion resistance (Ref 23, 24) of different materials from surface nanostructuring and work hardening of surface layer. Recent work on the tool steel AISI D2 showed much improvement in its wear resistance after combined laser heat treatment and ultrasonic impact treatment (Ref 25, 26). Peening of AISI 316 austenitic stainless steel with fine particles of Cr and Mo in N_2 atmosphere under controlled induction heating showed improved resistance against pitting corrosion in 3 wt.% $NaCl + H_2SO_4$ and 20 wt.% NaCl (Ref 27). The process of USSP on AA2024 and AA7150 alloys was found to increase the corrosion rate by 2-3 times because of contamination of the surface with Cu and Fe from the USSP treatment (Ref 28). However, the processing by USSP improved the localized corrosion resistance of these alloys (Ref 28, 29). The effect of USSP process on some orthopedic implant materials showed enhanced osteoblast proliferation owing to surface nanostructuring (Ref 30, 31), which is highly beneficial for orthopedic implants.

Some investigators have reported that SPD process can alter the microstructure of ferritic/martensitic (F/M) steels and enhance their mechanical properties (Ref 32-35). Ren et al. (Ref 36) and Zhe Liu (Ref 37) studied the effect of conventional shot peening and USSP, respectively, on corrosion behavior of F/M steels in supercritical water environment and found enhancement in corrosion resistance. However, there is no systematic study on the effect of USSP on microstructure and corrosion behavior of the modified 9Cr-1Mo Steel, in spite of liquid sodium or supercritical water being working environment for it in the nuclear reactors. In the present study, 100% NaCl coating was used for hot corrosion study because till date there are few literatures on the effect of (1) USSP and (2) USSP followed by pre-oxidation treatment on hot corrosion resistance of the modified 9Cr-1Mo steel in any environment. The present investigation deals with the effect of USSP treatment for different time periods on microstructure of the modified 9Cr-1Mo steel in normalized and tempered condition and on the effect of USSP treatment combined with subsequent pre-oxidation treatment on hot corrosion resistance under 100% NaCl coating. Significant improvement was observed in hot corrosion resistance of the modified 9Cr-1Mo steel under 100% NaCl coating following USSP and subsequent pre-oxidation treatment. It is also planned to study the effect of USSP with pre-oxidation on hot corrosion behavior of this steel in liquid sodium environment in future.

2. Experimental Procedure

2.1 Material

The modified 9Cr-1Mo steel was procured from the Indira Gandhi Center for Atomic Research (IGCAR), Kalpakkam, India, in the form of plate of $430 \times 203 \times 24$ mm^3 size in normalized and tempered (N & T) condition. Normalizing and tempering were carried out at 1050 and 770 °C, respectively. The nominal composition of the steel was 8.934 Cr, 0.862 Mo, 0.416 Mn, 0.206 V, 0.205 Ni, 0.200 Si, 0.109 C, 0.082 Nb, 0.064 Cu, 0.0517 N, 0.015 P, 0.010 Al, 0.004 Ti, 0.0008 S and balance Fe (wt.%).

2.2 Ultrasonic Shot Peening

Circular disks of 11.7 mm diameter and 4 mm thickness were prepared from the as-received plate and mechanically polished prior to USSP. The process of USSP was carried out by Stress Voyger SONATS using hard steel balls of 3 mm diameter, at amplitude of 80 μm and frequency of 20 kHz for different lengths of time (0.5, 1, 2.5 and 5 min). The samples USSPed for 0.5, 1, 2.5 and 5 min are designated as USSP0.5, USSP1, USSP2.5 and USSP5, respectively, and the as-polished sample (not subjected to USSP) is designated as Un-USSP.

2.3 Microstructure

Optical microstructure of the Un-USSP sample was examined following mechanical polishing and etching with Villela's reagent (1 g picric acid, 5 mL conc. HCl and 100 mL ethyl alcohol). The roughness of the shot peened surfaces was measured using profilometer (Mitutoyo SJ-410). The arithmetic mean roughness (Ra) was used to estimate the surface roughness of the USSPed samples. The shot peened specimens were sectioned along the thickness (normal to the shot peened surface) into two halves using a diamond-coated circular saw. The sectioned surfaces of the USSPed samples were examined under optical microscope and scanning electron microscope (FEI Quanta 200F). SEM examination was done also for the flat USSPed surfaces to analyze their morphology. EBSD (FEI NOVA NANO SEM 450) analysis was carried out at scan step size of 0.07 μm over the 100 μm × 100 μm area at a working distance of 15 mm and tilt angle of 70°. The sectioned samples were electrochemically polished in the electrolyte containing 20% perchloric acid in methanol, cooled to − 25 °C, at 25 V for 17 s, for EBSD study. TEM (Tecnai-G^2-T20) analysis was also carried out to assess grain refinement from USSP. The USSPed surface was sectioned perpendicular to thickness of the shot peened disk to a depth of 1 mm from the USSPed surface using a slow speed diamond-coated circular blade, and it was reduced to a thickness of 50 μm by polishing on emery paper. TEM foils were prepared by electrochemical polishing the electrolyte containing 6% perchloric acid and 34% n-butanol in methanol, cooled to − 38 °C, at 20 V, using a twin-jet electro-polisher (Struers Tenupol-5). X-ray diffractometer (Rigaku) with Cu Kα (λ = 0.1542 nm) radiation was used to determine phase constitution and crystallite size of the Un-USSPed and USSPed samples. The crystallite size (D) was calculated from diffraction line broadening of Bragg reflection of the peaks using the Scherrer equation, $D = 0.9 \ \lambda/\beta \ \cos\theta$, where θ is Bragg angle and β is peak broadening from grain refinement in the sample. Residual stresses were measured by $\sin^2\psi$ method using x-ray diffraction was carried out using the BRUKER D8 DISCOVER diffractometer with Cu Kα radiation and 2-mm-diameter collimator. Microhardness was measured using Shimadzu microhardness tester on the surfaces sectioned along the thickness (perpendicular to USSPed surface) from the USSPed surface to substrate, at an applied load of 50 g with dwell time of 10 s.

2.4 Hot Corrosion

For hot corrosion study, 100% NaCl was deposited by spray gun technique of the solution of 3.5 g NaCl in 100 mL distilled water, on the ultrasonic shot peened side of the circular disk specimens (11.7 mm diameter and 4 mm thickness) (Ref 38). While spraying, the samples were heated from underneath to a

temperature of ≈ 200 °C to remove moisture from the sprayed salt solution and deposit the salt. An amount of 5-7 mg/cm^2 of NaCl salt was deposited on the samples for the hot corrosion study. Sufficient care was taken during spraying to deposit the salt only on the USSPed surface and not on the other sides. This experiment was conducted for the Un-USSPed, USSPed and pre-oxidized USSPed samples.

Some USSPed samples were pre-oxidized at 600 °C for 4 h to study the effect of pre-oxidation of the USSPed samples on hot corrosion resistance. The designations of the samples used in this study are presented in Table 1. The NaCl-coated samples were exposed at 140 °C in an oven for 10 h for sticking of salt on the surface, and after that, they were placed in silica crucible in an electric resistance heating furnace at 600 °C for a period of 51 h in the normal air environment. Specimens were subjected to heating and cooling cycles with different time periods of exposure, initially for 2 h in each cycle of heating and cooling for the first three cycles, subsequently for 10 h in the next two cycles and finally for 25 h for the last cycle to a total duration of 51 h. Weight of the samples was measured after each cooling cycle. After completion of 51 h of exposure at 600 °C, XRD (Rigaku) analysis was carried out in the samples to analyze the products resulting from the hot corrosion in NaCl environment. The samples were also subjected to scanning electron microscopy and energy dispersive analysis by x-rays (EDAX) to examine the morphology and chemical composition of the oxide scale, respectively.

3. Results

3.1 Effect of USSP on Microstructure

3.1.1 Surface Morphology. The variation in surface roughness (Ra) with the duration of USSP is shown in Fig. 1. It is evident that the roughness of the USSPed surface is higher than that of the Un-USSPed surface. The roughness increases rapidly up to 0.5 and 1 min of USSP and remains nearly constant up to 5 min of USSP. The scanning electron micrographs of the USSPed surfaces are depicted in Fig. 2. It may be seen that there was overflow of material (marked by yellow arrow) in localized regions on surface of the specimens USSPed for longer durations of 2.5 and 5 min. There are also dark regions, marked by white arrow, resulting from level difference on the shot peened surface and the consequent shadowing effect.

3.1.2 Optical and SEM Analysis. Optical micrograph of the modified 9Cr-1Mo steel in the Un-USSP condition clearly reveals the prior austenite grain boundaries (PAGBs) (Fig. 3a), and the scanning electron micrograph shows precipitates along

the PAGBs as well within the grains (Fig. 3b). The optical and scanning electron micrographs of sectioned surfaces of the USSP5 specimen are shown in Fig. 4(a) and (b), respectively. Grain refinement may be seen in surface region of the USSP5 specimen, from both the micrographs.

3.1.3 TEM Analysis. Transmission electron micrograph of the Un-USSP P91 steel revealed lath martensite microstructure, with laths of less than 0.5 μm width and high density of dislocations. Some precipitates may be seen along the lath boundaries (marked by white arrow) (Fig. 5a). In general, this steel contains $M_{23}C_6$ (M = Cr, Fe), (25-250 nm) and MX ((V, Nb) (C, N)), (20-30 nm) in the N and T conditions (Ref 8). Owing to high dislocation density, there is a formation of sub-grain structure (encircled in Fig. 5a) with diameter of nearly 0.1 μm, within the lath martensite structure.

The bright-field images (Fig. 6a, b and c) of top surfaces of the samples USSPed for 0.5, 1 and 2.5 min revealed that lath martensitic structure was completely modified by the process of USSP. Owing to the severe strain induced by this process, there was a formation of nanosize grains with random crystallographic orientation, as evidenced by ring type diffraction pattern of the samples (Fig. 6A, B and C). However, the USSP0.5 sample did not show clear ring pattern as shown by the USSP1 and USSP2.5 samples. It might have happened due to un-developed nanostructure because of the lower strain induced during the short time period of USSP.

3.1.4 EBSD Analysis. Electron back-scattered diffraction analysis was carried out to characterize grain boundary orientation and quantify grain size of the both Un-USSPed and USSPed samples. The EBSD boundary map of the modified 9Cr-1Mo steel in the Un-USSP condition is presented in Fig. 7. It is evident that in the Un-USSPed condition this material contains boundaries with different angles of misorientation. Based on the misorientation, different colors are assigned to grain boundaries as mentioned in legend box in Fig. 7. In the present study, the grain boundaries with misorientation less than 15° are characterized as lath boundaries and with misorientation more than 15° are PAGBs. In general, misorientation difference between martensite variants ranges from 10° to 60° from Kurdjumov–Sachs (K–S) orientation relationship (Ref 39). However, it was observed that measured
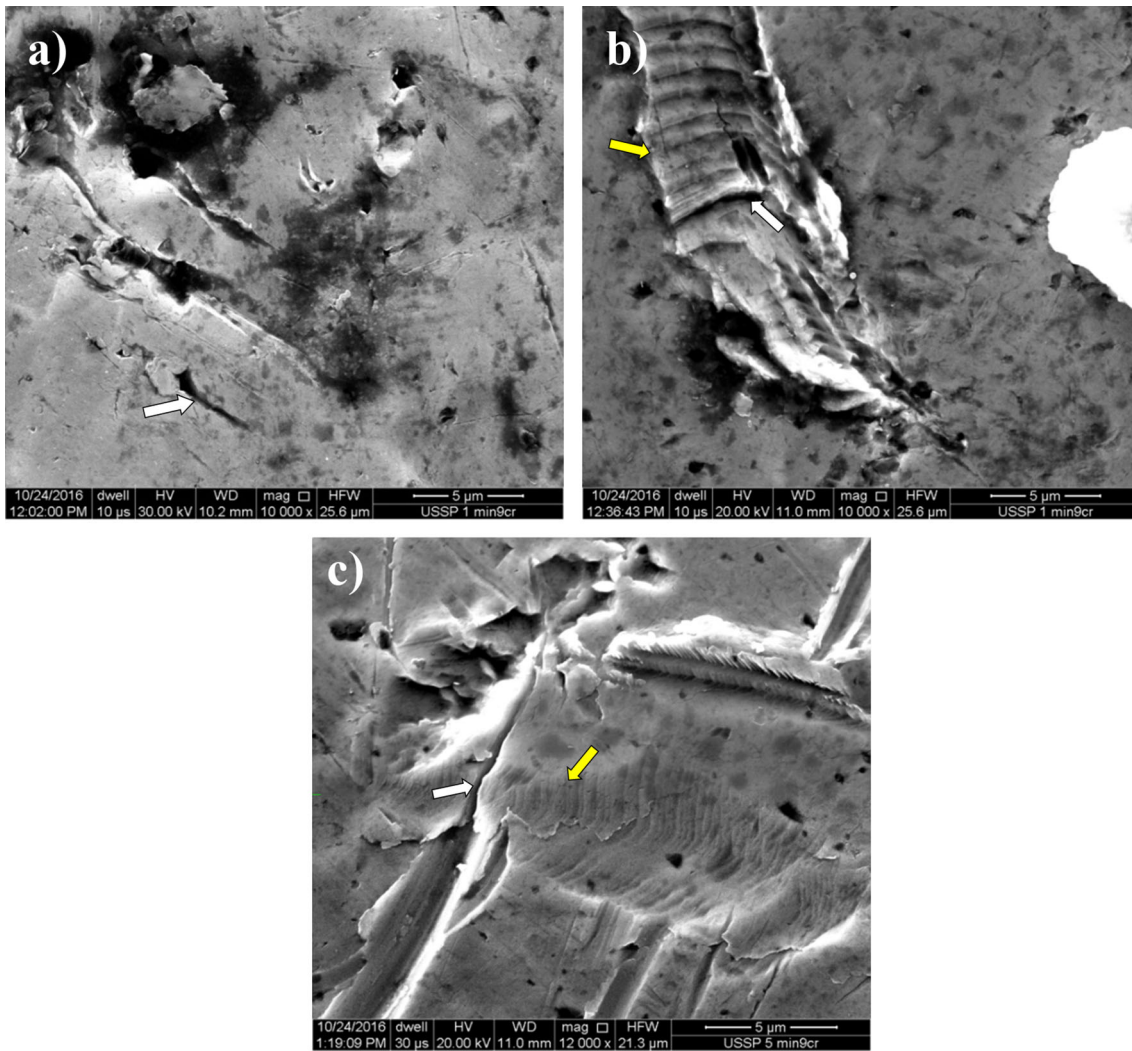
Table 1 Samples designation for hot corrosion study

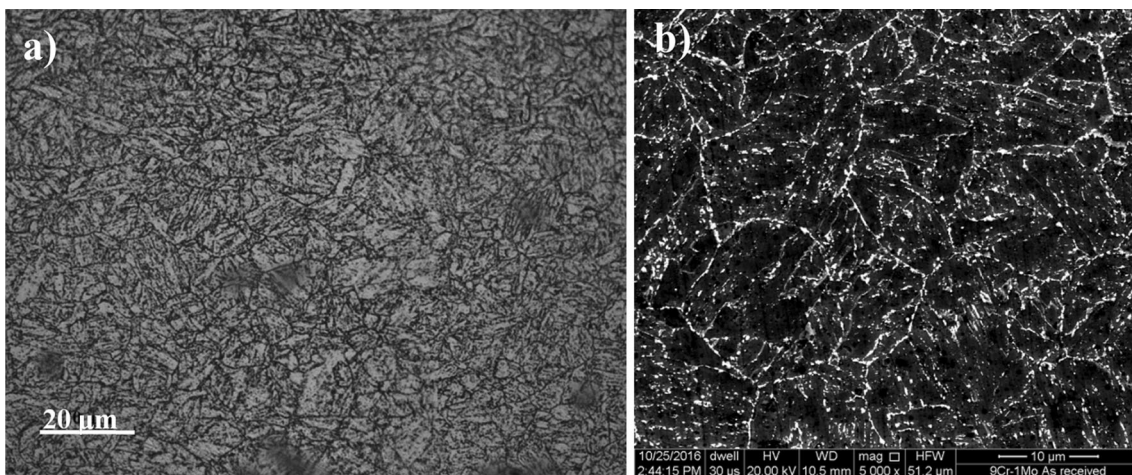| Sl. no	USSP time period, min	Oxidation treatment	Designation
1	0	No	Un-USSP
2	0.25	No	USSP0.25
3	1.5	No	USSP1.5
4	0.25	Yes	USSP0.25 + O
5	1.5	Yes	USSP1.5 + O
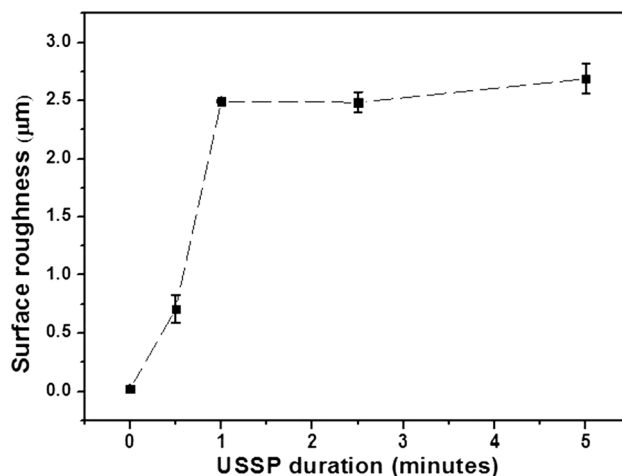
Fig. 1 Variation in the surface roughness (Ra) with the duration of USSP

Fig. 2 Surface morphology of the samples USSPed for (a) 1 min, (b) 2.5 min and (c) 5 min


Fig. 3 Microstructure of Un-USSPed sample. (a) Optical micrograph and (b) scanning electron micrograph

fraction of the high-angle lath boundaries was much less compared to the medium-angle boundaries (5°-10°) (Ref 40, 41); therefore, in the present study, low-angle boundaries ($< 15°$) are characterized as lath boundaries, neglecting low fraction of the high-angle boundaries. In order to determine grain size of the USSPed samples from EBSD analysis, grain
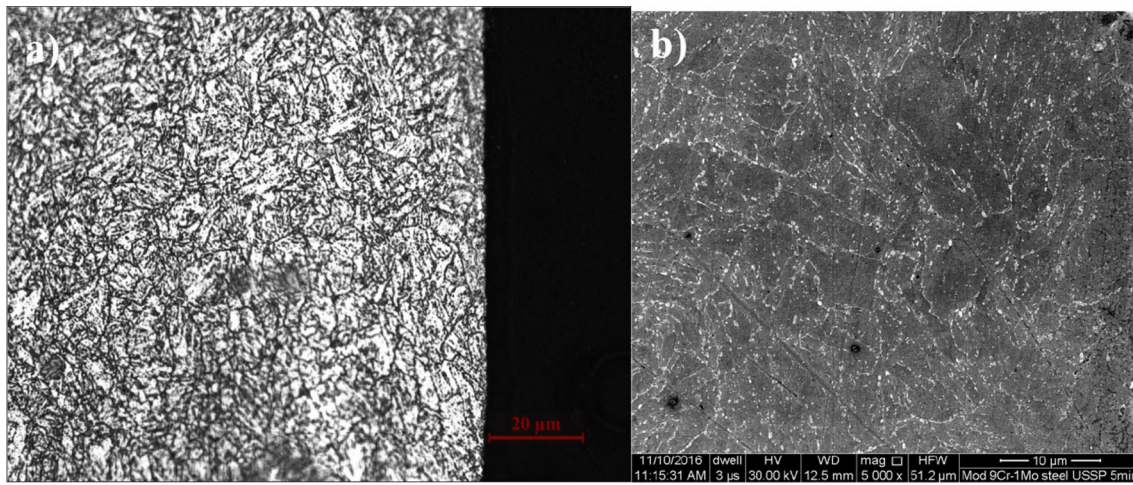
Fig. 4 Micrographs of sectioned surface of the USSP5 sample (right side of the image is the USSPed edge); (a) optical micrograph and (b) scanning electron micrograph
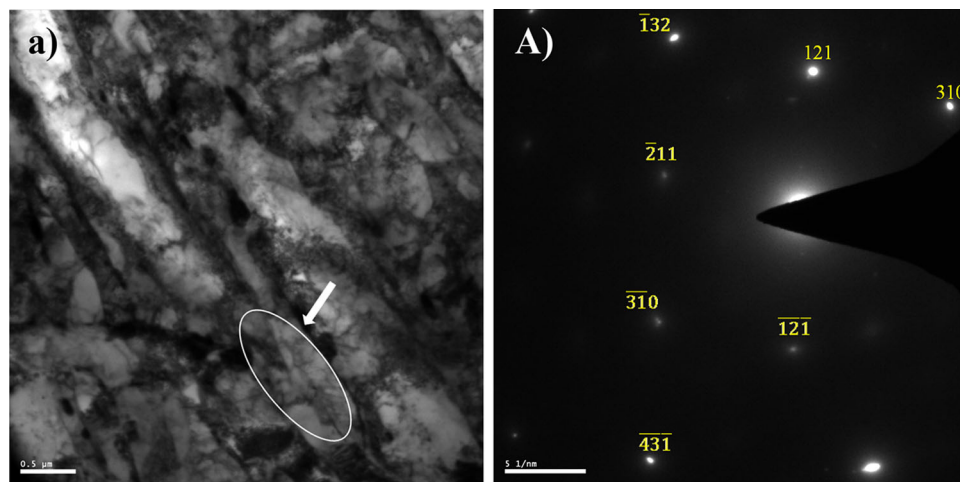
Fig. 5 Bright-field TEM image and the corresponding diffraction pattern of the Un-USSP sample

tolerance angle (GTA) as 5° was employed, assuming that the newly formed sub-grains from USSP have low-angle sub-grain boundaries. This assumption will also consider low-angle lath boundaries as sub-grains.

The image quality maps of sectioned surfaces of the Un-USSPed and USSPed samples are shown in Fig. 8. The fine-grained structure is clearly visible in the USSP2.5 (Fig. 8c) and USSP5 (Fig. 8d) conditions. In order to quantify misorientation of grain boundaries and grain size in the region of fine grains of the USSP2.5 and USSP5 samples, a dataset of $50 \times 50 \ \mu m^2$ area, close to the treated surface, was cropped and the distribution charts of grain size with grain tolerance angle of 5° and misorientations are depicted in Fig. 9 and 10, respectively. Figure 9 shows that the Un-USSPed sample contains grains of maximum diameter of 16 μm. Grain size chart of the USSP2.5 and USSP5 samples revealed that diameter of most of the grains was less than 2 μm and the area fraction of fine grains in the USSPed samples was higher than that of the Un-USSPed sample. Misorientation charts also showed that the USSP2.5 and USSP5 samples had higher number fraction of grain boundaries with misorientation angles in the range of 30°-60° as compared to that of the Un-USSPed sample.

3.1.5 XRD Analysis. The x-ray diffraction analysis revealed that there was no change in phase constitution of this steel following USSP and all the samples had body-centered cubic (BCC) crystal structure (Fig. 11). The average crystallite sizes calculated from the peak broadening were 78, 65 and 69 nm for the USSP1, USSP2.5 and USSP5 samples, respectively.

The magnified view of (110) peaks of the Un-USSPed and USSPed samples clearly show shifting of peaks to right side with respect to that of the Un-USSPed sample (Fig. 12), and shifting was more pronounced for the USSP5 sample. In general, uniform compressive strain in the material leads to decrease in interplanar spacing and therefore results in shifting of XRD peaks to high-angle sides (Ref 42). Figure 12 shows that USSP processing induced compressive strain into the surface of the material, and to quantify it, $\sin^2 \psi$ method was used in which residual stress is determined by measuring d-spacing at series of ψ tilts (Ref 43). The residual stress for the USSP5 condition was measured using XRD technique, and it was found that the USSP treatment for 5 min induced a compressive residual stress of 428 MPa in the surface region and these
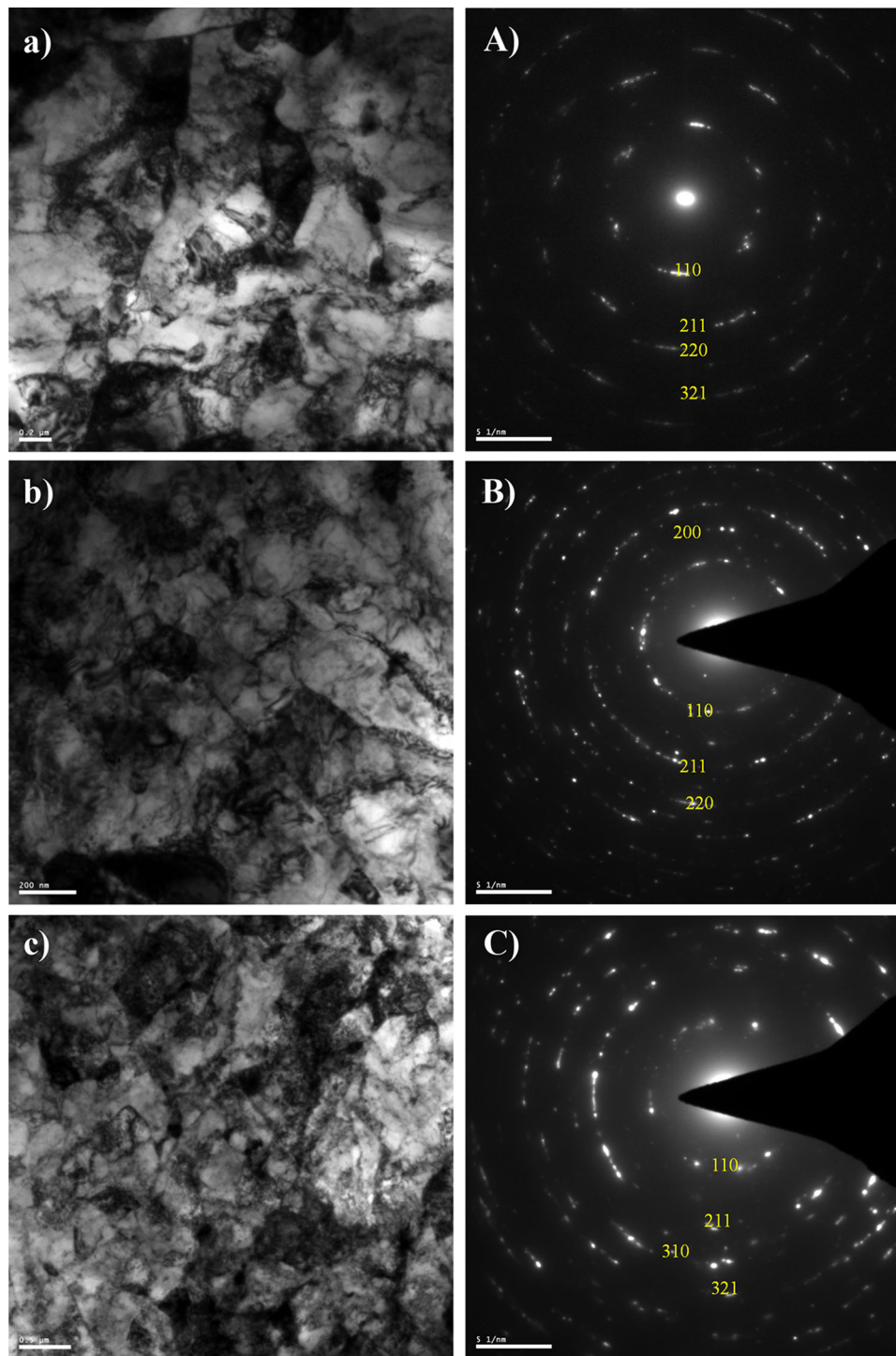
Fig. 6 Bright-field TEM images: (a) USSP0.5, (b) USSP1 and (c) USSP2.5 specimens; (A), (B) and (C) are their corresponding diffraction patterns

stresses were retained up to the depth of 250 μm depth (Fig. 13).

3.1.6 Microhardness. The microhardness of the modified 9Cr-1Mo steel in the Un-USSP condition is found to be 265 ± 4.1 VHN. The depthwise microhardness profiles of the USSP1 and USSP5 samples are presented in Fig. 14. It may be seen that USSP process enhanced the microhardness up to the depth of 65 μm from the USSPed edge to 300 ± 1.7 VHN

and there is a decrease in microhardness with increase in distance from the USSPed edge, which is very obvious phenomenon owing to gradient in strain distribution from the USSPed surface to the substrate level due to USSP. This increase in microhardness was attributed to severe work hardening due to increase in dislocation density, grain refinement and compressive residual stresses from the peened surface to several micron depths. There was no substantial
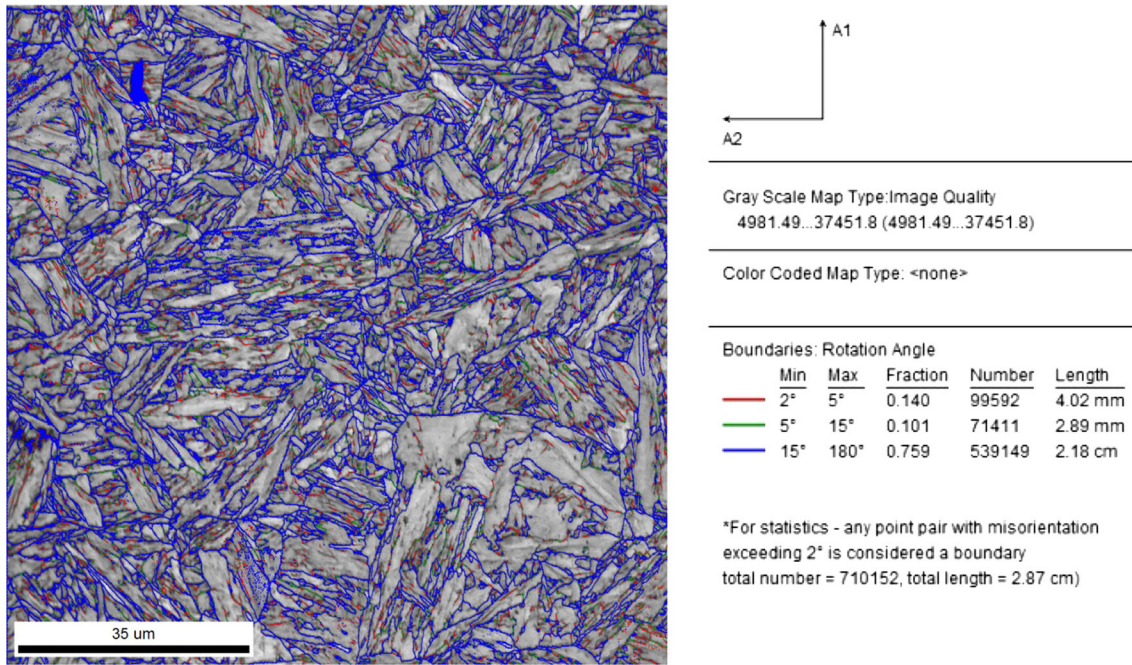
Fig. 7 EBSD boundary map of the Un-USSP modified 9Cr-Mo steel
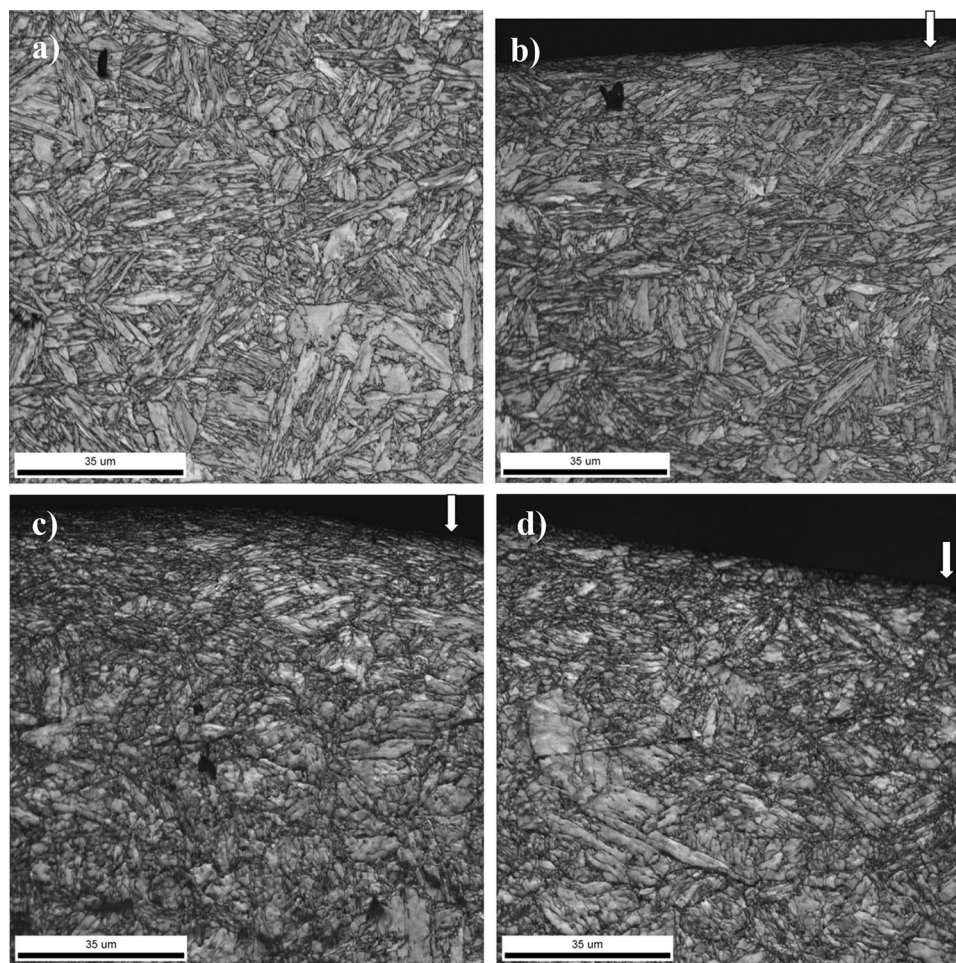
Fig. 8 EBSD image quality maps: (a) Un-USSP and sectioned surfaces (arrow represents the USSPed edge) of (b) USSP1, (c) USSP2.5 and (d) USSP5
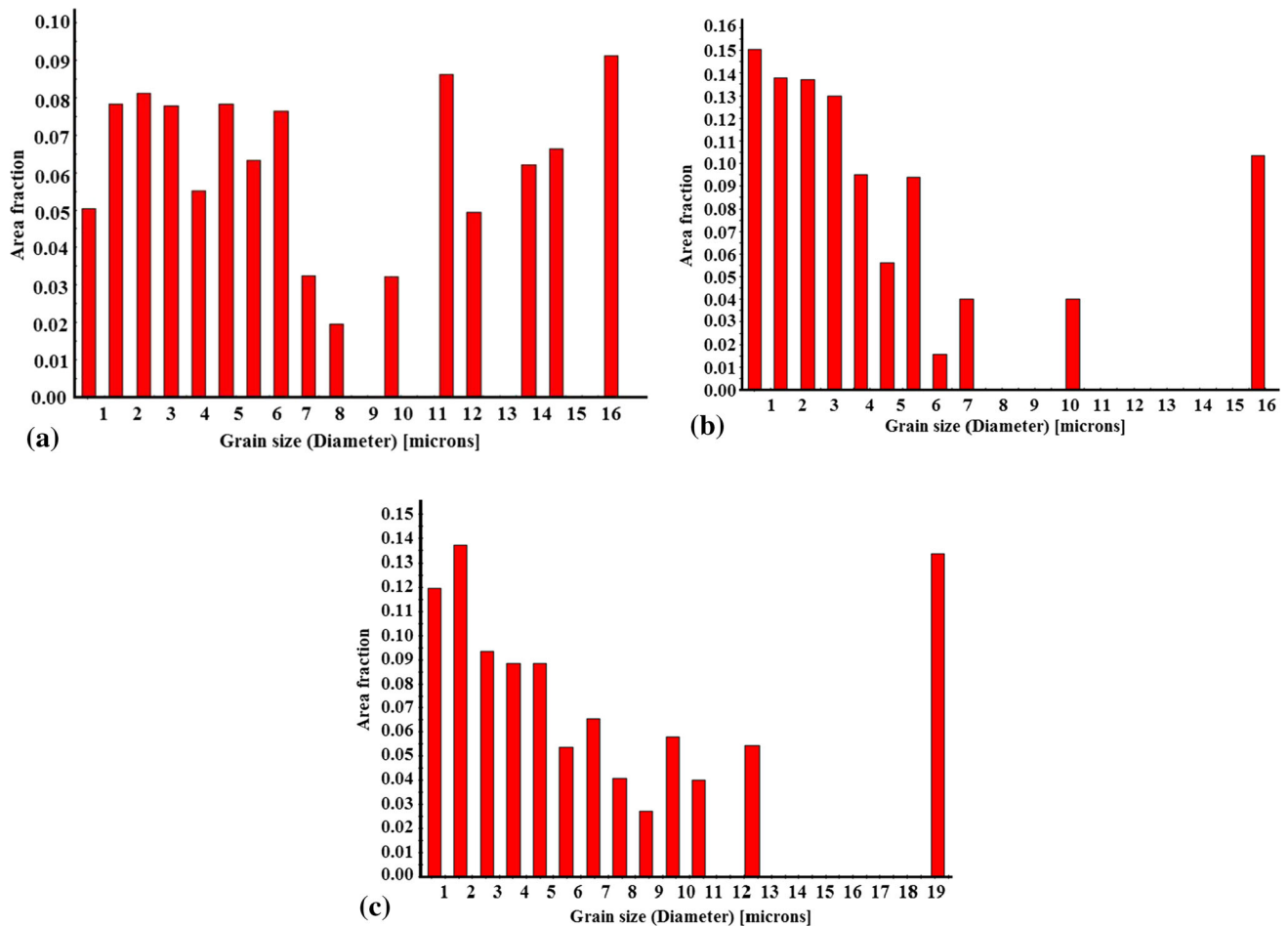
Fig. 9 Grain size distribution chart: (a) Un-USSP, (b) USSP2.5 and (c) USSP5 conditions

change in the microhardness with the duration of USSP at 65 μm depth. However, there is an appreciable change in the depth of the hardened layer with the time period of USSP, and USSP process of 1 min induced nearly 125-μm-deep work hardened layer, whereas USSP5 sample showed hardened layer of nearly 250 μm depth.

3.2 Effect of USSP on Hot Corrosion

3.2.1 Weight Gain Measurement. The variation in the square of weight gain per unit area into the 100% NaCl-coated sample, at 600 °C, up to 51 h of exposure, is shown in Fig. 15. Figure 15 shows that in the USSP and USSP combined with pre-oxidation, the USSP1.5 sample shows low weight gain per unit area than that of the 0.25-min USSPed sample, i.e., samples subjected to longer duration of USSP exhibit better resistance against hot corrosion than those subjected to less duration of USSP. However, sample only USSPed for 1.5-min duration and subsequently subjected to oxidation treatment at 600 °C showed lower weight gain per unit area than the Un-USSP sample, whereas the USSP0.25, USSP1.5 and USSP0.25 + O samples exhibited higher weight gain per unit area. It is also clear from the graph that corrosion kinetics followed the parabolic oxidation rate law as evident from the linear variation in the square of weight gain per unit area with the exposure time. The parabolic oxidation rate law is

expressed as, $W^2 = K_p t + C$, where W is weight gain per unit area (mg/cm^2), t is exposure time (hrs), K_p is parabolic rate constant (mg^2/cm^{4}h) and C is a constant. Corrosion behavior of the F/M steels studied by several researchers also revealed that corrosion kinetics followed parabolic rate law oxidation (Ref 44, 45).

The value of the parabolic rate constant, which is slope of the linear plot, is given in Table 2 along with the adj R^2, i.e., goodness of linear fit of the data points. The parabolic rate constant is also low for the USSP1.5 + O sample than that of the samples, i.e., modified 9Cr-1Mo steel USSPed for 1.5 min and oxidized for 4 h at 600 °C temperature showed better hot corrosion resistance at 600 °C in 100% NaCl atmosphere up to the exposure of 51 h.

3.2.2 Analysis of Oxide Scale. XRD analysis of the hot corrosion-tested samples for 51 h is depicted in Fig. 16. It is evident that corrosion products formed in the 100% NaCl environment at 600 °C consisted of several oxides of sodium and chromium.

SEM analysis of the oxide scale formed on all the samples subjected to hot corrosion test is presented in Fig. 17. Low-magnification SEM images (Fig. 17a, b, c, d and e) revealed surfaces with inhomogeneities and cracks (shown by arrow). The oxide scale seems to be smooth, and the severity of cracking is less in the case of USSP1.5 + O as compared to all the other samples. The EDS analysis revealed that corrosion
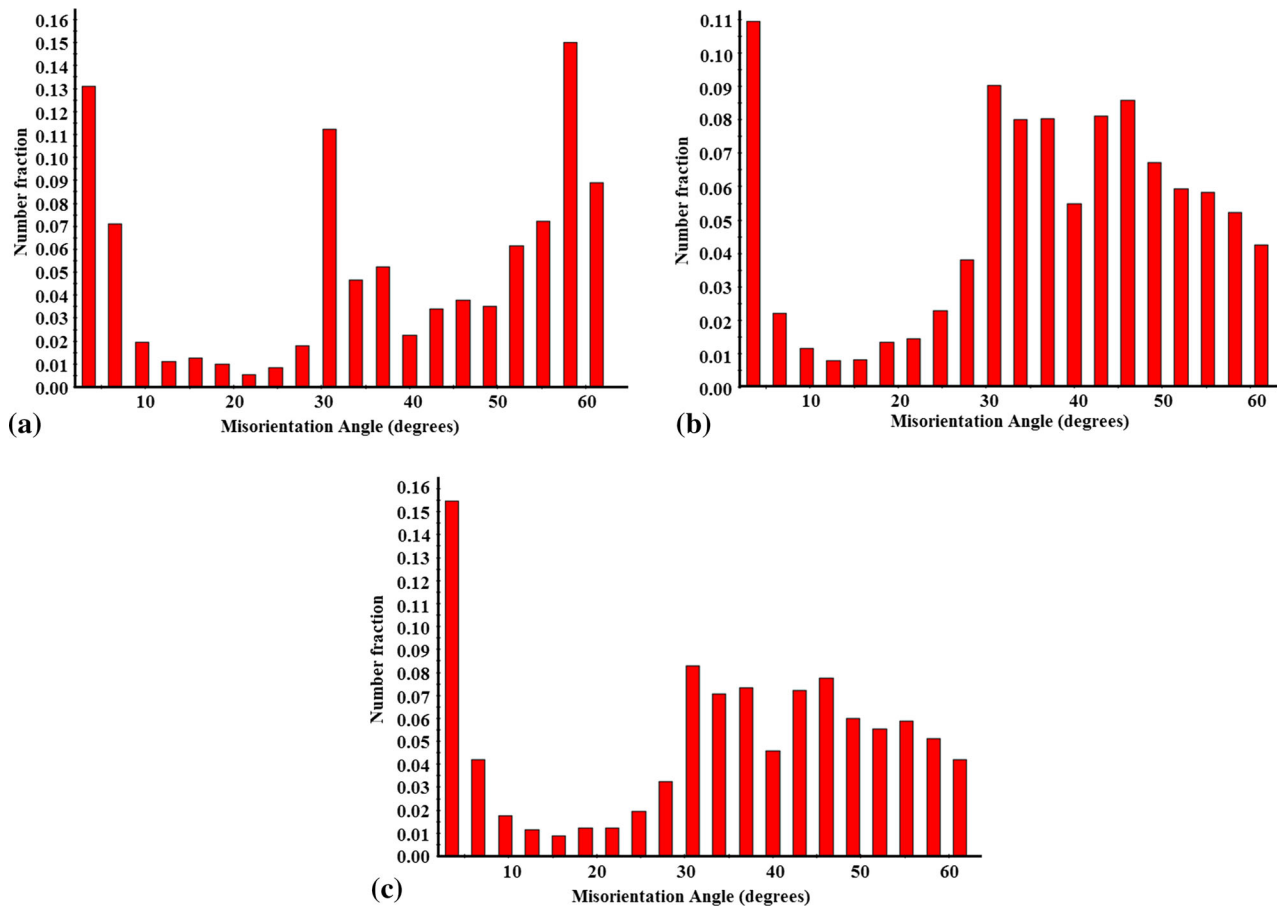
Fig. 10 Misorientation distribution chart for (a) Un-USSP, (b) USSP2.5 and (c) USSP5 conditions
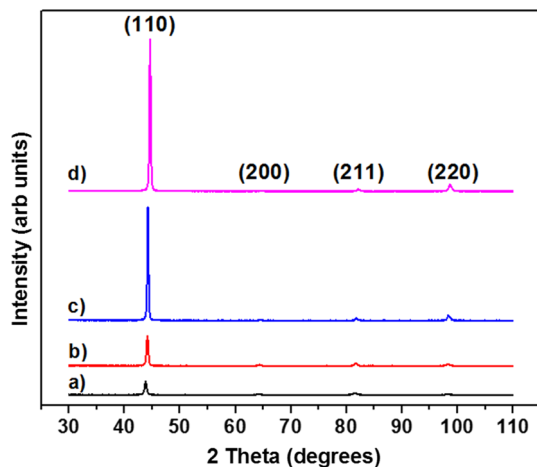

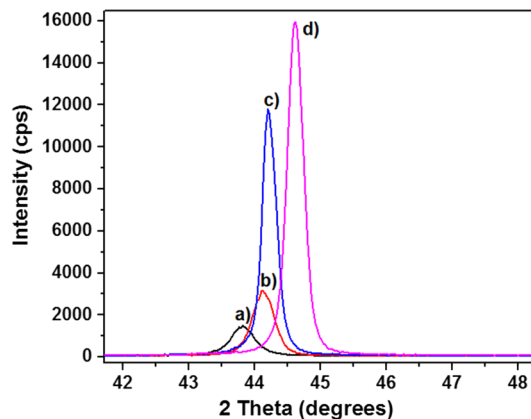**Fig. 11** XRD profiles of the (a) Un-USSP, (b) USSP1, (c) USSP2.5 and (d) USSP5 samples

Fig. 12 Magnified view of the 110 diffraction peaks of (a) Un-USSP, (b) USSP1, (c) USSP2.5 and (d) USSP5 conditions

product consisted mainly of the elements like Fe, Cr, O, Na and Cl and more or less the weight percents of the elements were similar in all the cases. The flaky morphology of oxide scale is revealed by the SEM micrographs at higher magnifications in all the samples subjected to hot corrosion test, as shown in Fig. 17(A), (B), (C), (D) and (E).

4. Discussion

4.1 Microstructure

In general, mechanism of grain refinement by USSP in a material depends on its stacking fault energy because of the change in the mode of deformation. It has been reported by
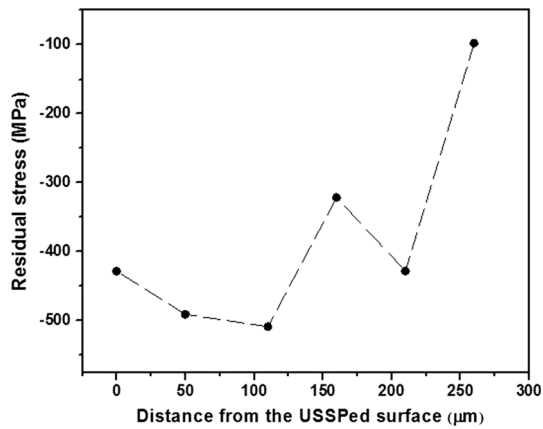
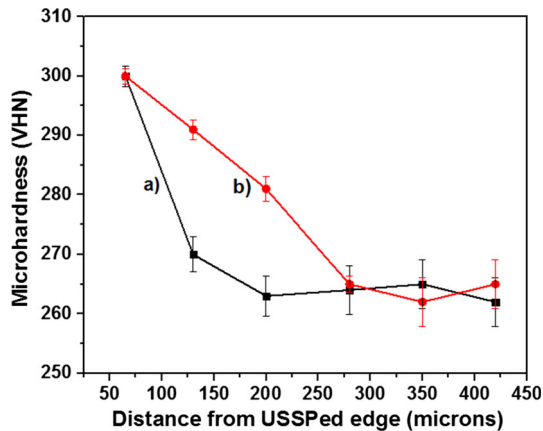**Fig. 13** Depth profile of residual stresses in USSP5 condition

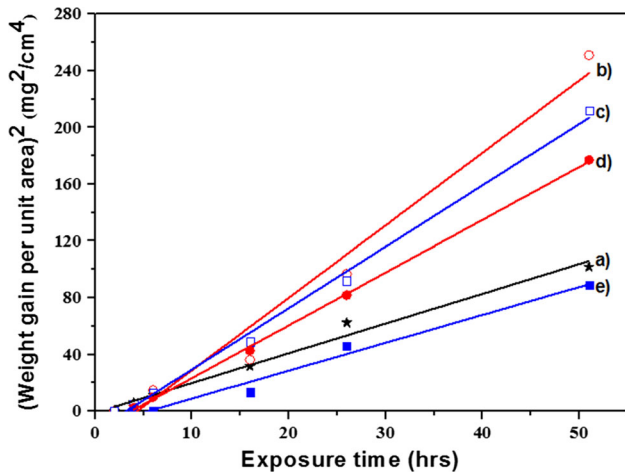**Fig. 14** Microhardness profiles of longitudinally sectioned samples (a) USSP1 and (b) USSP5

Fig. 15 Variation in the square of weight gain per unit area with exposure time in 100% NaCl at 600 °C for (a) Un-USSP, (b) USSP0.25, (c) USSP1.5, (d) USSP0.25 + O and (e) USSP1.5 + O

several investigators that modified 9Cr-1Mo steel has high stacking fault energy (Ref 46, 47). It has been established that owing to easy cross slip of dislocations in the high-stacking fault energy materials, dislocation-assisted mechanism leads to grain refinement (Ref 48-50). USSP is a kind of cold working

**Table 2 Parabolic rate constant (Kp) and goodness of linear fit values for hot corrosion-tested samples**

Sl. no	Condition	K_p, mg^2 cm^{-4} h^{-1}	adj R^2
1	Un-USSP	2.10129	0.983
2	USSP0.25	5.11381	0.970
3	USSP1.5	4.33146	0.995
4	USSP0.25 + O	3.72308	0.999
5	USSP1.5 + O	1.96897	0.978

process which increases the dislocation density and forms dislocation tangles. By virtue of interactions between dislocations, there is increase in the total strain energy, and to reduce it, tangled dislocation structure is rearranged into cellular substructure with dislocations as cell boundaries (Ref 51). In this way, there is continuous division of one grain into several cells which finally results in nanolevel grains at the surface, as demonstrated by the TEM bright-field images and the diffraction patterns (Fig. 6).

EBSD image quality map of the Un-USSP samples shows different types of grain boundaries (Fig. 7). As proposed by Ganesh et al. (Ref 52), the critical cooling rate to form complete martensitic structure in this steel is 4-5 K min^{-1}. The normalizing treatment led to the formation of lath martensitic structure in the austenite grains. Owing to good coherency between martensite laths and austenite, lath boundaries had low angle of misorientation, whereas there was more disorder at the PAGBs and the angle of misorientation was high (Ref 8). It was also confirmed by EBSD analysis that USSP process led to refinement of the grain structure and newly formed grains had diameter less than 2 μm and high misorientation. However, in this analysis nanosize grains were not observed, which may be due to restriction of grain tolerance angle (GTA) as 5° to determine the grain diameter. XRD results show that crystallite size decreased with USSP time period but higher durations of USSP led to slight increase in the crystallite size. This might be attributed to rise in temperature during USSP for longer time period which balances dislocation generation and recovery (Ref 53). There was discrepancy between the grain size measured from EBSD and crystallite size evaluated from XRD analysis, which may be attributed to dependence of grain size on GTA in the EBSD analysis and to coherent diffraction domain size in the XRD analysis.

Figure 11 shows that the intensity of the (110) peak was increased with USSP time period and it was highest for the USSP5. In general, intensity of diffraction peak solely depends on the number of crystallites in the material oriented in that direction, maintaining all the XRD operating parameters like the applied voltage, x-ray radiation and scanning rate to be constant. The increase in the intensity of (110) diffraction peak may be attributed to more number of crystals oriented in the direction of (110) in surface region of the USSPed samples. Regarding texture inducement by USSP process, there are contradictory reports in the literature. Blonde et al. (Ref 54) reported that severe texture in pulsed electro-deposited copper samples was randomized by USSP process, whereas Moering et al. (Ref 55) reported that USSP induced severe {110} texture in surface region of low-carbon steel. However, preferred crystallographic orientations in a material under deformation depend mainly on the magnitude of shear strain and shear
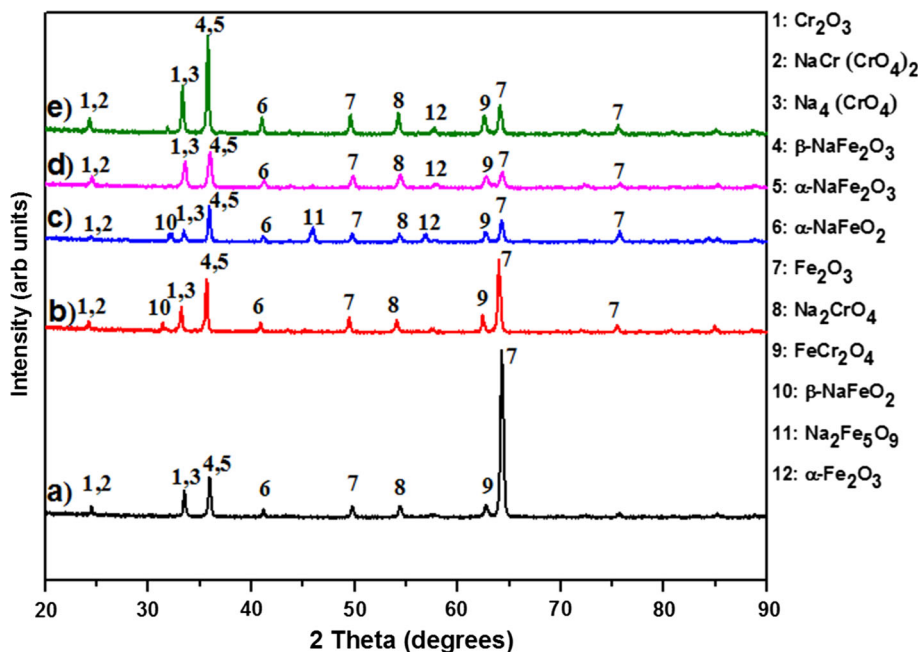
Fig. 16 XRD patterns of hot corroded samples following exposure of 51 h at 600 °C in 100% NaCl environment: (a) Un-USSP, (b) USSP0.25, (c) USSP1.5, (d) USSP0.25 + O and (e) USSP1.5 + O

direction. In order to increase the resolved shear stress, the slip planes in BCC material align parallel to shear direction and induce texture (Ref 55). Shifting of XRD peaks (Fig. 12) to right side with increase in the USSP duration might be due to decrease in the inter planar spacing because of compressive residual stresses induced by USSP (Ref 56). These residual stresses are created due to non-uniform deformation by USSP process, which produces both elastically and plastically deformed areas, so that plastically deformed material imposed constraint on elastically deformed material and induced residual stresses (Ref 57).

4.2 Hot Corrosion

It is well known that USSP process induced dislocations into surface region of material and increased its energy level as the dislocations were thermodynamically unstable. Thus, exposing the highly unstable surface to a reactive environment like 100% NaCl in the present case, the formation of protective chromium oxide layer was less favorable and the deleterious sodium and chlorine ions reacted with surface and subsequently reduced the corrosion resistance. In order to avoid it, the USSPed samples were subjected to oxidation treatment to form protective chromium oxide layer prior to hot corrosion test. This statement is proved valid through Fig. 15 of the present study, where only the USSP treated samples showed high weight gain per unit area than that of USSP and pre-oxidized samples, after subjecting to 100% NaCl environment at 600 °C. However, in the USSP + pre-oxidized samples also, only USSP1.5 + O showed good hot corrosion resistance than that of the Un-USSP sample but not the USSP0.25 + O. XRD patterns of USSP1.5 + O and USSP0.25 + O samples (Fig. 18) revealed that there was a formation of iron–chromium oxide layer on the surface after subjecting the USSP treated samples to oxidation treatment for 4 h at 600 °C. This discrepancy between hot corrosion resistances of the USSP0.25 + O and USSP1.5 + O

samples can be explained by morphology of the oxide scales formed on their surfaces.

Figure 19 shows scanning electron micrographs of surfaces of the samples (USSP0.25 + O and USSP1.5 + O) only subjected to pre-oxidation treatment. The morphology of the oxide scale formed on the USSP1.5 + O sample seems to be more uniform as compared to that formed on the USSP0.25 + O sample. Apart from the composition of the oxide scale, uniformity of the oxide scale plays an important role in enhancing the resistance against corrosive atmosphere. Due to better uniformity of the oxide scale on the USSP1.5 + O sample, it had better resistance against hot corrosion. The uniform iron–chromium oxide layer formed on the USSP1.5 + O sample, prior to salt spraying, acted as strong barrier for interaction between the corrosive environment and the material; thus, corrosion kinetics was reduced and there was less weight gain per unit area and the parabolic rate constant. The formation of more uniform oxide scale on the USSP1.5 + O as compared to that of the USSP0.25 + O sample can be explained from the bright-field TEM images. Figure 6(a, A) and (b, B) shows that USSP0.5 and USSP1 have un-developed and developed nanostructures, respectively. Thus, USSP0.25 sample may have un-developed, and the USSP1.5 sample has developed nanostructure. The grain boundary area fraction would be higher in the latter case than that of the former one which results in enhancement of diffusion of Cr from bulk to surface to ultimately result in the formation of uniform oxide scale in the USSP1.5 than that in the USSP0.25.

While the hot corrosion resistance of the USSP1.5 + O was higher than that of the Un-USSP, it was lower for the USSP1.5 and USSP0.25 than Un-USSP (Fig. 15). In general, USSP induces grain refinement in surface region and ultimately results in improvement of corrosion resistance owing to enhancement in diffusion of Cr to surface through grain boundaries created by USSP process. The reverse trend in the present study might be due to the fact that in Fe-Cr alloy
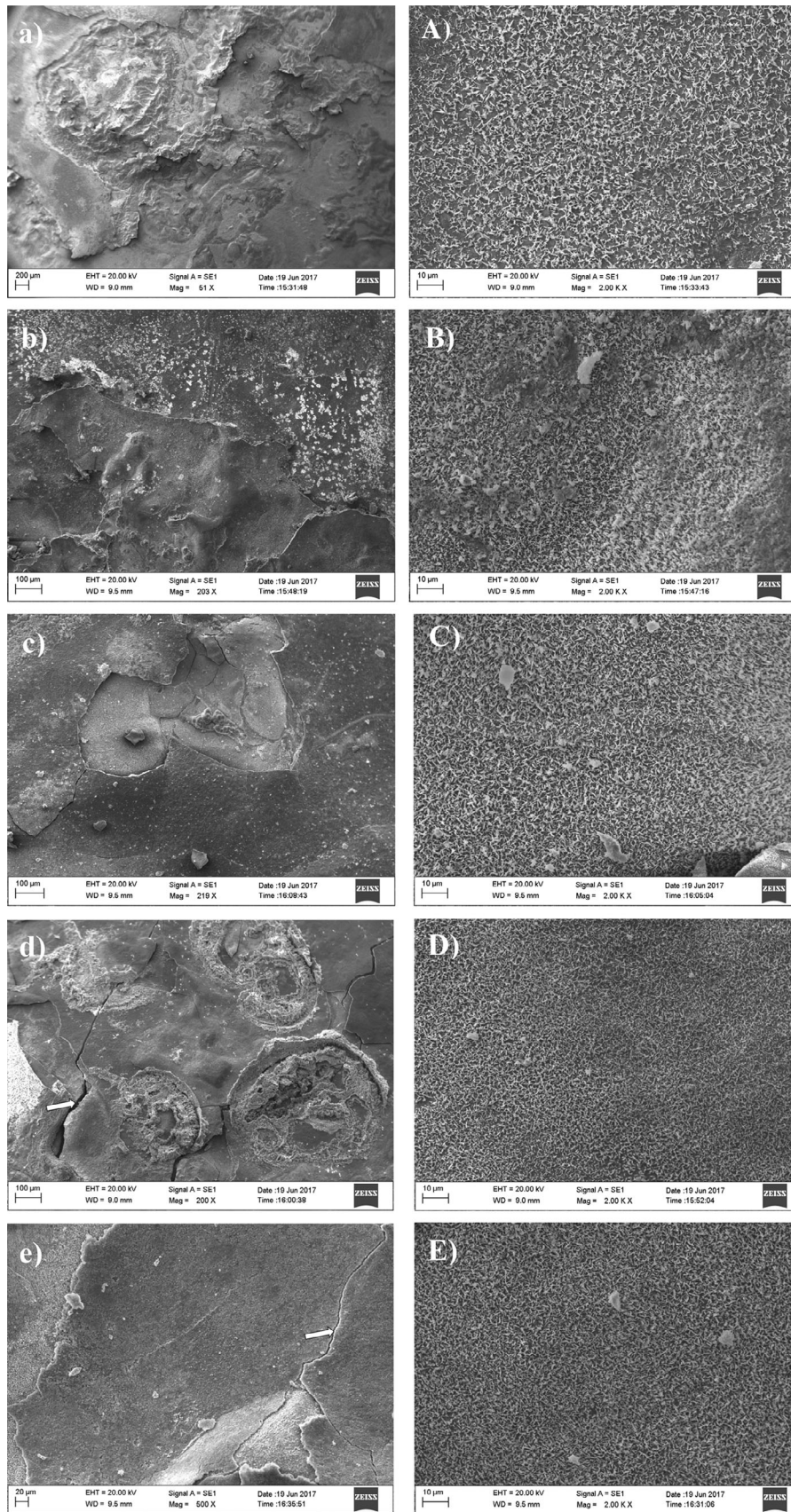
Fig. 17 SEM analysis of Un-USSP (a, A), USSP0.25 (b, B), USSP0.25 + O (c, C), USSP1.5 (d, D) and USSP1.5 + O (e, E) samples exposed to 100% NaCl at 600 °C for 51 h

systems the critical chromium content to form a protective continuous chromium oxide layer should be in the range of 13-20 wt.% (Ref 58), the modified 9Cr-1Mo steel used in this study contains only 8.934 wt.% of chromium as mentioned in section 2.1. Large number of grain boundaries induced by USSP increases the outward diffusion of both Fe and Cr to surface which results in the formation of iron–chromium oxide layer at the surface. This oxide layer is beneficial for hot corrosion resistance if it is rich in Cr content (Ref 36). Since the chromium content in this alloy is low, the oxide scale at the surface might be having high amount of Fe and less amount of Cr, which ultimately results in deleterious effect on hot corrosion resistance of the sample in 100% NaCl atmosphere. Relatively better hot corrosion resistance of the USSP1.5 than USSP0.25 might be attributed to somewhat higher Cr content at the surface oxide scale in the former than that in the latter, due to finer grain size in the USSP1.5 than in USSP0.25. Moreover, inhomogeneities observed in oxide scale of the hot corroded samples (Fig. 17) might be due to spallation of oxide scale during thermal cycling in hot corrosion test, and cracks in the

oxide scale (Fig. 17) are attributed to evaporation of chlorine ions/chlorides during exposure at high temperatures. It was also observed that optimum combination of the microstructure and crystallographic texture like off-basal and {110} texture led to enhancement of corrosion resistance of commercially pure titanium (Ref 59) in simulated body fluid and of the Zr-18% Nb alloys in 3.5% NaCl solutions (Ref 60). However, in the present study it was observed that {110} texture induced by the USSP treatment is not beneficial for hot corrosion resistance of the modified 9Cr-1Mo steel in 100% NaCl atmosphere. This may be attributed to the effect of exposure at elevated temperature during hot corrosion at 600 °C of the steel, due to which the texture developed from USSP at room temperature would have reduced and the hot corrosion resistance was not improved.

5. Conclusions

The following conclusions may be drawn from this study:

- Surface roughness of the modified 9Cr-1Mo steel was increased due to USSP.
- This USSP process completely modified the lath martensitic structure and induced nanosize grain structure in surface region of the steel without any change in the phase constitution.
- Quantitative EBSD analysis of the samples subjected to USSP process showed that grains of diameter less than 2 μm with high grain boundary misorientation were induced in surface region of the normalized and tempered modified 9Cr-1Mo steel.
- The depth of the work hardened layer was found 275 μm with 13% increase in the microhardness and compressive residual stress of 420 MPa was induced in surface region of the USSP5 specimen.
- Hot corrosion resistance of the modified 9Cr-1Mo steel in 100% NaCl environment at 600 °C was improved by prior USSP for 1.5 min and subsequent oxidation treatment at 600 °C for 4 h owing to surface grain refinement and formation of effective protective iron–chromium oxide layer.
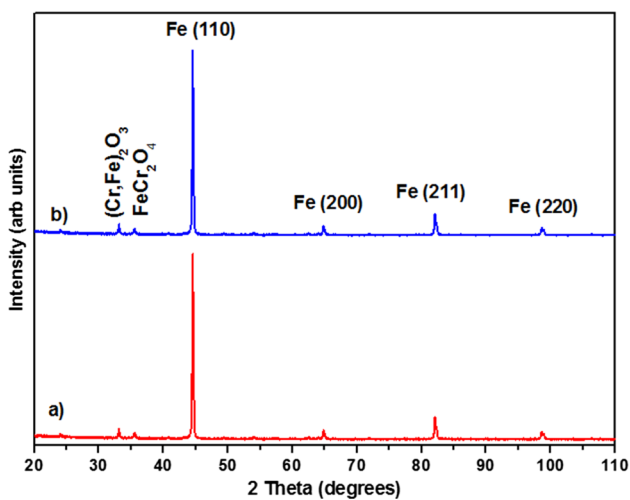
Fig. 18 XRD patterns of the (a) USSP0.25 and (b) USSP1.5 samples after 4-h oxidation at 600 °C
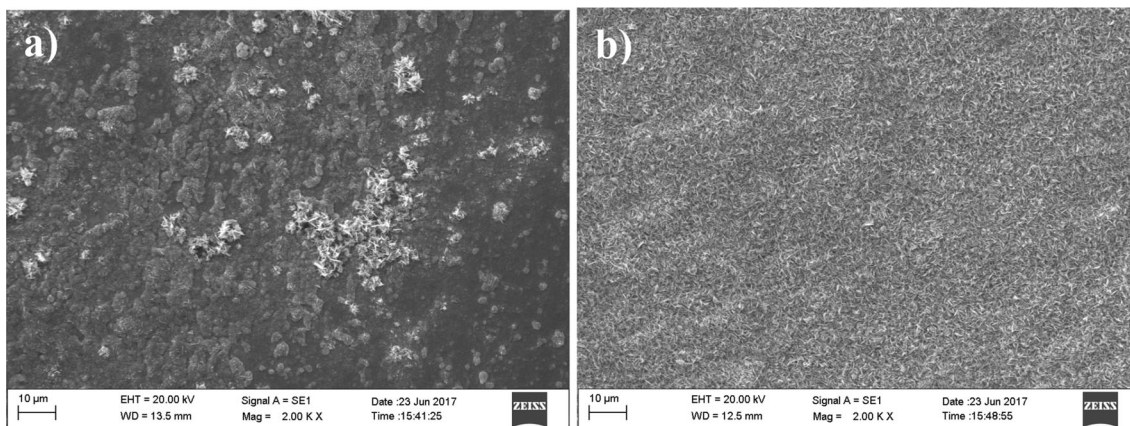
Fig. 19 SEM images of surface: (a) USSP0.25 + O and (b) USSP1.5 + O samples

References

1. S.L. Mannan, S.C. Chetal, B. Raj, and S.B. Bhoje, Selection of Materials for Prototype Fast Breeder Reactor, *Trans. Indian Inst. Met.*, 2003, **56**(2), p 155–178

2. R.L. Klueh and A.T. Nelson, Ferritic/Martensitic Steels for Next-Generation Reactors, *J. Nucl. Mater.*, 2007, **371**(1), p 37–52

3. T. Shrestha, S.F. Alsagabi, I. Charit, G.P. Potirniche, and M.V. Glazoff, Effect of Heat Treatment on Microstructure and Hardness of Grade 91 Steel, *Metals*, 2015, **5**(1), p 131–149

4. W.B. Jones, C.R. Hills, and D.H. Polonis, Microstructural Evolution of Modified 9Cr-1Mo Steel, *Metall. Mater. Trans. A*, 1991, **22**(5), p 1049–1058

5. A. Kumar, B.K. Choudhary, K. Laha, T. Jayakumar, K.B.S. Rao, and B. Raj, Characterisation of Microstructure in 9% Chromium Ferritic Steels Using Ultrasonic Measurements, *Trans. Indian Inst. Met.*, 2003, **56**(5), p 483–497

6. S.H. Kim, W.S. Ryu, and I.H. Kuk, Microstructure and Mechanical Properties of Cr-Mo Steels for Nuclear Industry Applications, *Nucl. Eng. Technol.*, 1999, **31**(6), p 561–571

7. V.K. Sikka, Development of Modified 9Cr1Mo Steel for Elevated-Temperature Service, in *Topical Conference on Ferritic Alloys for Use in Nuclear Energy Technologies*, ed. by J.W. Davis and D.L. Michel, (Snowbird, UT, 1983)

8. V.T. Paul, S. Saroja, and M. Vijayalakshmi, Microstructural Stability of Modified 9Cr–1Mo Steel During Long Term Exposures at Elevated Temperatures, *J. Nucl. Mater.*, 2008, **378**(3), p 273–281

9. F. Benjamin, S. Maxime, R. Alexandra, B. Françoise, and P. André, Microstructural Evolutions and Cyclic Softening of 9% Cr Martensitic Steels, *J. Nucl. Mater.*, 2009, **386**, p 71–74

10. B. Fournier, M. Sauzay, F. Barcelo, E. Rauch, A. Renault, T. Cozzika, L. Dupuy, and A. Pineau, Creep-Fatigue Interactions in A 9 pct Cr-1 pct Mo Martensitic Steel: Part II. Microstructural Evolutions, *Metall. Mater. Trans. A*, 2009, **40**(2), p 330–341

11. D.W. Kim and S.S. Kim, Contribution of Microstructure and Slip System to Cyclic Softening of 9 wt% Cr Steel, *Int. J. Fatigue*, 2012, **36**(1), p 24–29

12. J. Singh and D.E. Wolfe, Review Nano and Macro-structured Component Fabrication by Electron Beam-Physical Vapor Deposition (EB-PVD), *J. Mater. Sci.*, 2005, **40**(1), p 1–26

13. S.B. Fard and M. Guagliano, Effects of Surfaces Nanocrystallization Induced by Shot Peening on Material Properties: A Review, *Frattura ed Integrità Strutturale*, 2009, **7**, p 3–16

14. Y. Samih, B. Beausir, B. Bolle, and T. Grosdidier, In-Depth Quantitative Analysis of the Microstructures Produced by Surface Mechanical Attrition Treatment (SMAT), *Mater. Charact.*, 2013, **83**, p 129–138

15. K. Lu and J. Lu, Nanostructured Surface Layer on Metallic Materials Induced by Surface Mechanical Attrition Treatment, *Mater. Sci. Eng., A*, 2004, **375**, p 38–45

16. Y.H. Wei, B.S. Liu, L.F. Hou, B.S. Xu, and G. Liu, Characterization and Properties of Nanocrystalline Surface Layer in Mg Alloy Induced by Surface Mechanical Attrition Treatment, *J. Alloys Compd.*, 2008, **452**(2), p 336–342

17. Y.M. Xing and J. Lu, An Experimental Study of Residual Stress Induced by Ultrasonic Shot Peening, *J. Mater. Process. Technol.*, 2004, **152**(1), p 56–61

18. M. Ya, Y. Xing, F. Dai, K. Lu, and J. Lu, Study of Residual Stress in Surface Nanostructured AISI, 316L Stainless Steel Using Two Mechanical Methods, *Surf. Coat. Technol.*, 2003, **168**(2), p 148–155

19. T. Balusamy, T.S. Narayanan, K. Ravichandran, I.S. Park, and M.H. Lee, Influence of Surface Mechanical Attrition Treatment (SMAT) on the Corrosion Behaviour of AISI, 304 Stainless Steel, *Corros. Sci.*, 2013, **74**, p 332–344

20. A.L. Ortiz, J.W. Tian, L.L. Shaw, and P.K. Liaw, Experimental Study of the Microstructure and Stress State of Shot Peened and Surface Mechanical Attrition Treated Nickel Alloys, *Scr. Mater.*, 2010, **62**(3), p 129–132

21. T. Watanabe, K. Hattori, M. Handa, N. Hasegawa, K. Tokaji, M. Ikeda, and J.M. Duchazeaubeneix, Effect of Ultrasonic Shot Peening on Fatigue Strength of High Strength Steel, in *Proc. ICSP8, Garmisch-Partenkirchen*, ed. by L. Wagner, (2002), pp. 305–310

22. V. Pandey, K. Chattopadhyay, N.S. Srinivas, and V. Singh, Low Cycle Fatigue Behavior of AA7075 with Surface Gradient Structure Produced by Ultrasonic Shot Peening, *Procedia Struct. Integr.*, 2016, **2**, p 3288–3295

23. T. Balusamy, S. Kumar, and T.S. Narayanan, Effect of Surface Nanocrystallization on the Corrosion Behaviour of AISI, 409 Stainless Steel, *Corros. Sci.*, 2010, **52**(11), p 3826–3834

24. V. Pandey, J.K. Singh, K. Chattopadhyay, N.S. Srinivas, and V. Singh, Influence of Ultrasonic Shot Peening on Corrosion Behavior of 7075 Aluminum Alloy, *J. Alloys Compd.*, 2017, **723**, p 826–840

25. D.A. Lesyk, S. Martinez, B.N. Mordyuk, V.V. Dzhemelinskyi, A. Lamikiz, G.I. Prokopenko, YuV Milman, and K.E. Grinkevych, Microstructure Related Enhancement in Wear Resistance of Tool Steel AISI, D2 by Applying Laser Heat Treatment Followed by Ultrasonic Impact Treatment, *Surf. Coat. Technol.*, 2017, **328**, p 344–354

26. D.A. Lesyk, S. Martinez, B.N. Mordyuk, V.V. Dzhemelinskyi, A. Lamikiz, G.I. Prokopenko, K.E. Grinkevych, and I.V. Tkachenko, Laser-Hardened and Ultrasonically Peened Surface Layers on Tool Steel AISI, D2: Correlation of the Bearing Curves' Parameters, Hardness and Wear, *J. Mater. Eng. Perform.*, 2018, **27**(2), p 764–776

27. S. Kikuchi, S. Iwamae, H. Akebono, J. Komotori, and K. Kadota, Effect of Atmospheric-Controlled Induction-Heating Fine Particle Peening on Electrochemical Characteristics of Austenitic Stainless Steel, *Surf. Coat. Technol.*, 2018, **334**, p 189–195

28. Q. Sun, X. Liu, Q. Han, J. Li, R. Xu, and K. Zhao, A comparison of AA2024 and AA7150 Subjected to Ultrasonic Shot Peening: Microstructure, Surface Segregation and Corrosion, *Surf. Coat. Technol.*, 2018, **337**, p 552–560

29. Q. Sun, Q. Han, R. Xu, K. Zhao, and J. Li, Localized Corrosion Behaviour of AA7150 After Ultrasonic Shot Peening: Corrosion depth vs. Impact Energy, *Corros. Sci.*, 2018, **130**, p 218–230

30. Y. Guo, B. Hu, C. Tang, Y. Wu, P. Sun, X. Zhang, and Y. Jia, Increased Osteoblast Function In Vitro and In Vivo through Surface Nanostructuring by Ultrasonic Shot Peening, *Int. J. Nanomed.*, 2015, **10**, p 4593–4603

31. J. Havlikova, J. Strasky, M. Vandrovcova, P. Harcuba, M. Mhaede, M. Janecek, and L. Bacakova, Innovative Surface Modification of Ti–6Al–4 V Alloy with a Positive Effect on Osteoblast Proliferation and Fatigue Performance, *Mater. Sci. Eng., C*, 2014, **39**, p 371–379

32. Z.Q. Fan, T. Hao, S.X. Zhao, G.N. Luo, C.S. Liu, and Q.F. Fang, The Microstructure and Mechanical Properties of T91 Steel Processed by ECAP at Room Temperature, *J. Nucl. Mater.*, 2013, **434**(1), p 417–421

33. M. Eddahbi, M.A. Monge, T. Leguey, P. Fernández, and R. Pareja, Texture and Mechanical Properties of EUROFER 97 Steel Processed by ECAP, *Mater. Sci. Eng., A*, 2011, **528**(18), p 5927–5934

34. D.C. Foley, K.T. Hartwig, S.A. Maloy, P. Hosemann, and X. Zhang, Grain Refinement of T91 Alloy by Equal Channel Angular Pressing, *J. Nucl. Mater.*, 2009, **389**(2), p 221–224

35. P. Fernández, M. Eddahbi, M.A. Auger, T. Leguey, M.A. Monge, and R. Pareja, Microstructural and Mechanical Characteristics of EUROFER'97 Processed by Equal Channel Angular Pressing, *J. Nucl. Mater.*, 2011, **417**(1), p 20–24

36. X. Ren, K. Sridharan, and T.R. Allen, Effect of Grain Refinement on Corrosion of Ferritic–Martensitic Steels in Supercritical Water Environment, *Mater. Corros.*, 2010, **61**(9), p 748–755

37. Z. Liu, Corrosion Behavior of Designed Ferritic-Martensitic Steels in Supercritical Water, Doctoral Dissertation, University of Alberta (Canada) (2013)

38. G.S. Mahobia, Neeta Paulose, and Vakil Singh, Hot Corrosion Behavior of Superalloy IN718 at 550 and 650 C, *J. Mater. Eng. Perform.*, 2013, **22**(8), p 2418–2435

39. S. Morito, H. Tanaka, R. Konishi, T. Furuhara, and A.T. Maki, The Morphology and Crystallography of Lath Martensite in Fe-C Alloys, *Acta Mater.*, 2003, **51**(6), p 1789–1799

40. Z. Lv, X. Zhang, X. Huang, and N. Hansen, EBSD Characterization of Deformed Lath Martensite in IF Steel, *IOP Conf. Ser. Mater. Sci. Eng.*, 2017, **219**(1), p 012033–012039

41. P.K. Parida, A. Dasgupta, and S. Saibaba, Study of Microstructure and Microtexture of Modified 9Cr–1Mo Steel Subjected to High Deformation, *J. Nucl. Mater.*, 2013, **432**(1–3), p 450–454

42. D. Cullity, *Elements of X-Ray Diffraction*, Morris Cohen ed., Addison-Wesley Publishing Company, Boston, 1956

43. P.J. Withers, Residual Stresses: Measurement by Diffraction, *Encyclopedia of Materials: Science and Technology*, 2nd ed., K.H.J. Buschow, R.W. Cahn, M.C. Flemings, B. Ilschner, E.J. Kramer, S. Mahajan, and P. Veyssiere, Eds., Elsevier, 2001, p 8158-8169

44. D. Laverde, T. Gomez-Acebo, and F. Castro, Continuous and Cyclic Oxidation of T91 Ferritic Steel Under Steam, *Corros. Sci.*, 2004, **46**(3), p 613–631

45. V. Singh, J.S. Kachhawaha, and V.B. Tare, Corrosion Behavior of 9Cr-1Mo Steel in Sulfur Dioxide Environment, *J. Mater. Eng. Perform.*, 2014, **23**(9), p 3285–3298

46. J. Christopher, B.K. Choudhary, E.I. Samuel, V.S. Srinivasan, and M.D. Mathew, Tensile Flow and Work Hardening Behaviour of 9Cr–1Mo Ferritic Steel in The Frame Work of Voce Relationship, *Mater. Sci. Eng., A*, 2011, **528**(21), p 6589–6595

47. D. Samantaray, C. Phaniraj, S. Mandal, and A.K. Bhaduri, Strain Dependent Rate Equation to Predict Elevated Temperature Flow Behavior of Modified 9Cr-1Mo (P91) Steel, *Mater. Sci. Eng., A*, 2011, **528**(3), p 1071–1077

48. X. Wu, N. Tao, Y. Hong, B. Xu, J. Lu, and K. Lu, Microstructure and Evolution of Mechanically-Induced Ultrafine Grain in Surface Layer of Al-Alloy Subjected to USSP, *Acta Mater.*, 2002, **50**(8), p 2075–2084

49. N.R. Tao, Z.B. Wang, W.P. Tong, M.L. Sui, J. Lu, and K. Lu, An Investigation of Surface Nanocrystallization Mechanism in Fe Induced by Surface Mechanical Attrition Treatment, *Acta Mater.*, 2002, **50**(18), p 4603–4616

50. Z.G. Liu, H.J. Fecht, and M. Umemoto, Microstructural Evolution and Nanocrystal Formation During Deformation of Fe–C Alloys, *Mater. Sci. Eng., A*, 2004, **375**, p 839–843

51. D.G. Ellwood and D.J. Bacon, *Mechanical Metallurgy*, Vol Vol, McGraw-Hill, New York, 1986, p 3

52. B. Jeya Ganesh, S. Raju, A. Kumar Rai, E. Mohandas, M. Vijayalak-shmi, K.B.S. Rao, and B. Raj, Differential Scanning Calorimetry Study of Diffusional and Martensitic Phase Transformations in Some 9 Wt% Cr Low Carbon Ferritic Steels, *Mater. Sci. Technol.*, 2011, **27**(2), p 500–512

53. N.R. Tao, M.L. Sui, J. Lu, and K. Lua, Surface Nanocrystallization of Iron Induced by Ultrasonic Shot Peening, *Nanostruct. Mater.*, 1999, **11**(4), p 433–440

54. R. Blonde, H.L. Chan, N. Allain-Bonasso, B. Bolle, T. Grosdidier, and J. Lu, Evolution of Texture and Microstructure in Pulsed Electro-Deposited Cu Treated by Surface Mechanical Attrition Treatment (SMAT), *J. Alloys Compd.*, 2010, **504**, p S410–S413

55. J. Moering, X. Ma, G. Chen, P. Miao, G. Li, G. Qian, S. Mathaudhu, and Y. Zhu, The Role of Shear Strain on Texture and Microstructural Gradients in Low Carbon Steel Processed by Surface Mechanical Attrition Treatment, *Scr. Mater.*, 2015, **108**, p 100–103

56. P.S. Prevey, Current Applications of X-Ray Diffraction Residual Stress Measurement, *Developments in Materials Characterization Technologies*, ASM International, Materials Park, OH, 1996, p 103–110

57. M. Kobayashi, T. Matsui, and Y. Murakami, Mechanism of Creation of Compressive Residual Stress by Shot Peening, *Int. J. Fatigue*, 1998, **20**(5), p 351–357

58. M.S. El-Basiouny and S. Haruyama, The Polarization Behaviour of FeCr Alloys in Acidic Sulphate Solutions in the Active Region, *Corros. Sci.*, 1976, **16**(8), p 529–540

59. N.P. Gurao, G. Manivasagam, P. Govindaraj, R. Asokamani, and S. Suwas, Effect of texture and Grain Size on Bio-corrosion Response of Ultrafine-Grained Titanium, *Metall. Mater. Trans. A*, 2013, **44**(12), p 5602–5610

60. N.I. Khripta, O.P. Karasevska, and B.N. Mordyuk, Surface Layers of Zr-18% Nb Alloy Modified by Ultrasonic Impact Treatment: Microstructure, Hardness and Corrosion, *J. Mater. Eng. Perform.*, 2017, **26**(11), p 5446–5455